


## Research Article

# Preliminary Investigation of the Potentialities of a Mesoscale Meteorological Model to Reproduce Experimental Statistics of Rain Attenuation on Earth-Space Links

Laurent Castanet <sup>1</sup>, Valentin Le Mire,<sup>1</sup> Julien Queyrel,<sup>1</sup> Xavier Boulanger,<sup>2</sup>  
and Laurent Féral<sup>3</sup>

<sup>1</sup>ONERA/DEMR, Université de Toulouse, Toulouse, France

<sup>2</sup>Instrumentation, Telemetry/Telecommand & Propagation Division, CNES, France

<sup>3</sup>Laboratoire d'Aérodynamique, Université Toulouse 3, Toulouse, France

Correspondence should be addressed to Laurent Castanet; [laurent.castanet@onera.fr](mailto:laurent.castanet@onera.fr)

Received 29 November 2021; Revised 1 July 2022; Accepted 29 July 2022; Published 6 October 2022

Academic Editor: Giuseppe Castaldi

Copyright © 2022 Laurent Castanet et al. This is an open access article distributed under the Creative Commons Attribution License, which permits unrestricted use, distribution, and reproduction in any medium, provided the original work is properly cited.

Current spatial resolutions achieved by mesoscale weather forecast models allow them to be used to generate the state of the lowest layers of the atmosphere over areas as small as a few square kilometers which corresponds to the typical size of the tropospheric area crossed by Earth-space links. Furthermore, they allow the evolution of the troposphere to be predicted with a time stamp of five minutes instead of every hour with large-scale weather forecast models which makes them attractive for radio propagation predictions for satellite communication applications. This paper aims at studying the capability of the Weather Research and Forecast (WRF) model coupled with an electromagnetic physical model to reproduce rain attenuation statistics for Earth-space paths at Ka-band. To this purpose, one year of propagation measurements collected at 20 GHz in different places at midlatitudes in Toulouse and Salon de Provence (France), Spino d'Adda (Italy), Aveiro (Portugal), and Madrid (Spain), at high latitudes in Svalbard (Norway) and at low latitudes in Kourou are used to make comparisons between simulations and measurements. Comparisons between the simulated and the experimental annual statistics considered in this paper provide encouraging results, with a similar accuracy as Recommendation ITU-R P.618-13 for midlatitude European locations and with better accuracy for a high latitude area in Svalbard and for an equatorial location in French Guiana.

## 1. Introduction

Nowadays, fixed satellite communication systems deliver services everywhere in the world to provide access to the Internet with higher and higher data rates for the consumer to communicate or to use any kinds of multimedia applications at any time. Experiencing increasing success, these satellite systems have been widely developed using available standard technologies at Ku-band for big satellites placed in geostationary orbit. As a consequence of this success, before being deployed new satellite systems shall demonstrate that they will not cause interference to existing ones, through sharing studies controlled by the regulator: the International Telecommunication Union. These sharing studies impose a lot of constraints on antenna patterns and on power

amplifiers to avoid harmful interference, so much so that the complexity of the systems will increase a lot and it will then be more convenient to use a higher frequency band where more spectrum is available, even if the technology is more expensive. Therefore, the combined needs for the end users to benefit from higher data rates and the regulatory rules are now resulting in the observed tendency to go to higher frequency bands such as Ka band (20–30 GHz) [1], Q/V band (40–50 GHz) [2] or probably W-band (70–80 GHz) in the future [3, 4].

On the other hand, the maturity of the technology allows designers to propose new systems using non-GSO orbits and several projects of satellite constellations have appeared recently, constituted of tens of medium size satellites in MEO orbits [5] or of hundreds or thousands of small

satellites in LEO orbits [6]. In addition, high frequency datalinks are needed not only for telecommunications but also to transfer data from Earth observation satellites or from scientific missions in near Earth or in deep space.

However, with increasing frequencies, the impact of the Earth's atmosphere will degrade the propagation of transmitted signals due to attenuation (by gases, clouds, and rain), scintillation due to tropospheric turbulence or depolarization due to nonspherical particles on the path [7]. To close link budgets, that is to specify the appropriate margin to be considered to comply with service availability, it is necessary to know the statistics of these propagation effects. For more than 50 years, a lot of prediction methods of propagation impairments have been proposed in the open literature and the reference method to be followed to predict total impairments for Earth-space paths is given in Recommendation ITU-R P.618 [8]. More recently in the last 20 years, channel models have been developed allowing time series of propagation impairments to be synthesized in order to optimize by preliminary simulating the system design and operation through the use of fade mitigation techniques [9] such as power control, adaptive waveform, or site diversity. The reference channel model is described in Recommendation ITU-R P.1853 [10].

Today, statistical prediction methods and channel models have been tested for links established with GEO satellites thanks to propagation campaigns performed with GEO satellites, such as ACTS [11] in the US, Olympus [12], Italsat [13], and Alphasat [14] in Europe, or the ETS series in Japan [15]. However, to upgrade them for non-GSO configurations, only very few propagation experiments have been performed so far and their duration was not sufficient to obtain reliable statistics. Indeed, for a LEO configuration, a single satellite can be seen from a reference Earth station only around 10 to 15 min per day, which represents a number of samples 100 times lower than with a GEO configuration. Therefore, if 5 years are needed to obtain reliable propagation statistics with a GEO experiment, the number of years needed to obtain meaningful annual statistics with a LEO satellite would be significantly higher. So other solutions have to be found to develop and test propagation models for non-GSO configurations.

A new approach to replace propagation campaigns could be to use a physical description of the atmosphere and to convert it into propagation attenuation. In a first attempt, the use of the UK Met'Office Unified Model was proposed [16] to generate the atmosphere and then to apply physical models to produce rain attenuation time series. The main drawback of this approach was the poor resolution of the rain attenuation time series: 5 km in space and 1 hour in time. Considering the progress of computational power and storage capacity, a promising solution would be in a first step to use high resolution mesoscale meteorological weather forecast models to generate the spatial-temporal behavior of the troposphere. Then, in a second step this evolving volume would be converted into propagation parameters thanks to physical models of the interaction between an electromagnetic wave and the atmospheric medium, such as radiative transfer equation (RTE), turbulence theory, or Mie theory [17, 18].

In a recent past, the use of mesoscale models with RTE proved to be appropriate to model clear sky propagation conditions with the MM5 model to perform link budget for deep space links [19] or for radio links with GEO satellites. In parallel, [18, 20–22] Outeiral et al., Jeannin et al., and Fayon et al. propose to use this type of approach to model rain attenuation whose variability in space and in time is significantly faster than oxygen and water vapor attenuation. However, if these preliminary results are quite promising, the validation of the method describing the behavior of rain attenuation on the long-term (that is in terms of local Complementary Cumulative Distribution Functions (CCDFs) of rain attenuation) has not been proved yet in the open literature.

Therefore, the objective of this paper is to show how a mesoscale weather forecast model used in reanalysis mode, coupled with a physical model relying on the Mie theory of scattering can be successfully used to predict long-term CCDFs of rain attenuation. In Section 2, the use of the Weather Research and Forecast (WRF) model coupled with an electromagnetic module (EMM) is described. The propagation data used to test the representativeness of the model are presented in Section 3. Finally, Section 4 shows the comparisons between the simulations and the statistics generated from propagation measurements collected in several types of climates.

## 2. Coupling of a Mesoscale Meteorological Model with an Electromagnetic Module

*2.1. Overview of WRF.* WRF is a mesoscale numerical weather prediction system which can simulate atmospheric states using real data or idealized conditions [23]. In this paper, the high-resolution numerical weather prediction model WRF-ARW (v3.4) is used in reanalysis mode to generate a 4D description of the atmosphere at high temporal (5 min) and spatial (2 km) resolutions, thus computing data cubes in a horizontal square of approximately  $160 \times 160 \text{ km}^2$  and using 36 vertical levels of atmosphere up to 20 km height. WRF is initialized using the ECMWF ERA-Interim reanalysis database which provides surface and pressure levels parameters every 6 hours with a horizontal resolution of  $0.75 \times 0.75^\circ$  (around  $85 \times 85 \text{ km}^2$ ) [24]. ERA-Interim data are also used by WRF-ARW as boundary conditions every 6 hours.

Atmospheric data such as temperature, pressure, humidity, and wind profiles are downloaded from ERA-Interim for the desired time period and for the desired region around a central point defined by its geographic coordinates (longitude and latitude), as shown in Figure 1. This information is used to provide sufficiently detailed boundary conditions to WRF in order to solve the Navier–Stokes equations that describe the dynamics of the atmosphere and the related thermodynamic equations.

In order to synthesize realistic past states of the atmosphere, simulations are limited to one day with a previous 12-hour spin-up period (the results of which are deleted later on) giving the opportunity for the model to provide stable outputs. In order to reach the  $2 \times 2 \text{ km}^2$  horizontal

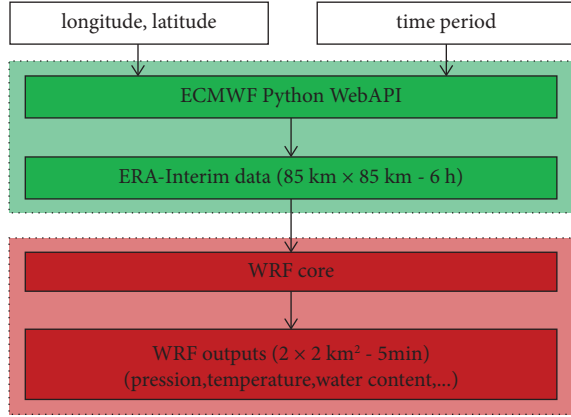


FIGURE 1: Block diagram of the WRF-ARW simulation.

resolution, three nested domains are used: a coarser domain with a  $30 \times 30 \text{ km}^2$  resolution on a polar stereographic projection and static fields initialized directly through an interpolation from ERA-Interim, and two successive nests at  $6 \times 6 \text{ km}^2$  and  $2 \times 2 \text{ km}^2$  resolution (see Table 1 and Figure 2).

As the solving of such equations requires detailed modelling of the various energy fluxes and of the phase changes, the WRF model includes different models to represent energy transfers between atmospheric layers. Among the parameters computed by WRF, the following ones are of interest to calculate rain attenuation: the pressure level  $P$  expressed in Pa, the temperature  $T$  in K, and the precipitating liquid water specific content  $Q_r$  in kg/kg (mass of precipitating water per kg of air mass).

**2.2. Electromagnetic Module (EMM).** At the output of WRF-ARW simulation, a 4D volume of tropospheric parameters is produced that are converted into propagation parameters and more particularly into rain attenuation using an electromagnetic module (EMM) developed at ONERA (see Figure 3).

The specific attenuation due to rain,  $\gamma_r$  in dB/km, is derived from the following equation (25):

$$\gamma_r = 0.4343 \int_0^{D_{\max}} \sigma_{\text{ext}}(D) N(D) dD, \quad (1)$$

where  $\sigma_{\text{ext}}(D)$  in  $\text{cm}^2$  is the extinction cross-section,  $N(D)$  in  $\text{cm}^{-4}$  is the rain drop size distribution per class of diameter, and  $D_{\max}$  in cm is the diameter of the largest raindrop (generally around 0.6 or 0.8 cm because raindrops larger than this size tend to break up when colliding with other large raindrops).

Assuming rain drops as spherical particles, the extinction cross section  $\sigma_{\text{ext}}(D)$  in  $\text{cm}^2$  can be computed using Mie's theory [26, 27], which inherently assumes spherical rain drops. As larger drops tend to be oblate spheroids, alternative method such as point matching technique would be better suited, in particular when depolarization needs to be studied.

The rain drop size distribution  $N(D)$  is derived from the expression of the modified gamma distribution [28]:

$$N(D) = N_0 D^\mu e^{-\Lambda D}, \quad (2)$$

where  $\Lambda$  is the slope parameter and  $\mu$  is the shape parameter of the modified gamma distribution.

The slope parameter  $\Lambda$  depends on the precipitating water content  $M_r$  in  $\text{kg/m}^3$  as

$$\Lambda = \left( \frac{\pi \rho_w N_0 \Gamma(\mu + 4)}{6 M_r} \right)^{1/\mu+4}, \quad (3)$$

where  $\rho_w$  is the density of water in  $\text{kg/m}^3$  ( $\rho_w = 997 \text{ kg/m}^3$ ) and  $\Gamma$  is the gamma distribution function.

An example of the impact of  $\mu$  parameter on rain attenuation is presented in for an equatorial area. The number of input parameters to be fixed can be reduced assuming a Marshall–Palmer raindrop size distribution [29], so that

$$N_0 = 0.08 \text{ cm}^{-4} \mu = 0. \quad (4)$$

Therefore, the only missing information is the precipitating water content  $M_r$ . It is related to the precipitating water mixing ratio  $Q_r$  given by WRF for each pixel cube (in kg/kg) [30] through the following formula:

$$M_r = Q_r \rho_d, \quad (5)$$

where  $\rho_d$  is the dry air density (in  $\text{kg/m}^3$ ) expressed from the dry air pressure  $P_d$  in Pa and the temperature  $T$  in K as

$$\rho_d = \frac{P_d}{R_d T}, \quad (6)$$

where the specific gas constant for dry air  $R_d = 287.058 \text{ J kg}^{-1} \text{ K}^{-1}$ .

Once the specific attenuation due to rain  $\gamma_r$  is calculated at the considered frequency for each pixel of the d03 domain (horizontal resolution  $2 \times 2 \text{ km}^2$ ), the  $\gamma_r$  values are integrated along the path length to compute rain attenuation time series for the considered (azimuth and elevation angles) satellite radio-link until a specific attenuation value of 0 dB/km is reached.

Azimuth  $\varphi$  and elevation  $\theta$  angles are calculated from the following equations:

$$\varphi = \arctan\left(\frac{\tan(L_{es} - L_s)}{\sin(l_{es})}\right) + 180(^{\circ}),$$

$$\theta = \arctan\left(\frac{\cos(l_{es}) \cos(L_{es} - L_s) - R_E + h/R_E + h + R_s}{\sqrt{1 - (\cos(l_{es}) \cos(L_{es} - L_s))^2}}\right)^{\circ}, \quad (7)$$

where  $L_{es}$ ,  $l_{es}$ , and  $h$  are the longitude, the latitude, and the altitude, respectively, amsl (above mean sea level) of the Earth station,  $L_s$  is the satellite longitude on the geostationary orbit,  $R_E$  is the mean radius of the Earth, and  $R_s$  is the satellite altitude.

In order to avoid boundary effects, the d03 domain is truncated from 11 pixels at each side of the grid, and the actual size of the d03 domain is therefore  $102 \times 102 \text{ km}^2$ . For all locations except SvalSat, the station is placed at the centre of the d01 domain; for the extreme case of SvalSat where a

TABLE 1: WRF domain resolutions.

Domains	Spatial resolutions	Temporal resolutions	Grid sizes
d01 (outer nest)	$30 \times 30 \text{ km}^2$	1 hour	$1710 \times 1710 \text{ km}^2$
d02 (middle nest)	$6 \times 6 \text{ km}^2$	1 hour	$480 \times 480 \text{ km}^2$
d03 (inner nest)	$2 \times 2 \text{ km}^2$	5 min	$156 \times 156 \text{ km}^2$

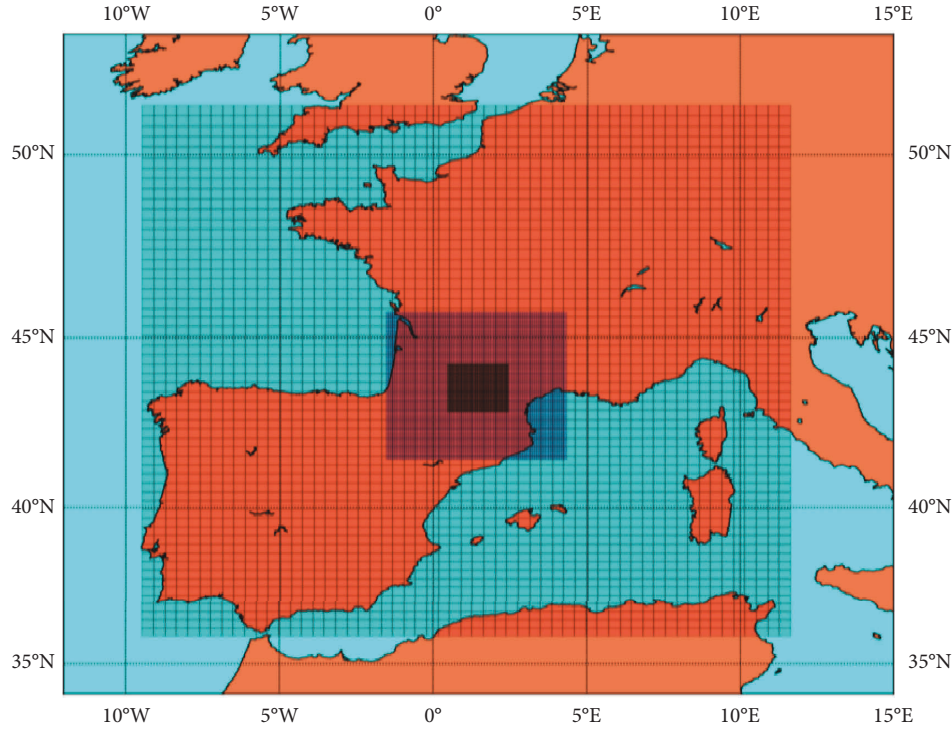


FIGURE 2: Illustration of the three nested geographical domains of the WRF-ARW simulation.

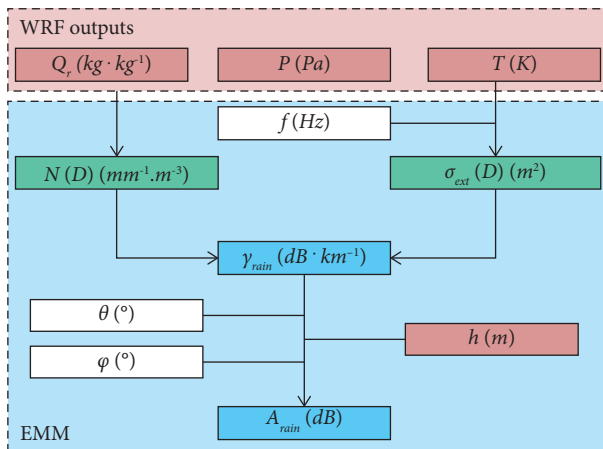


FIGURE 3: Overview of the EMM from the outputs generated by WRF.

very low elevation is considered ( $2.65^\circ$ ), the station is shifted to have the middle of the path length (up to the  $0^\circ\text{C}$  isotherm height) placed at the centre of the d01 domain.

For the considered simulation duration, the computation of rain attenuation is performed every five minutes.

### 3. The Reference Database

In order to parametrize and test the simulator (particularly the electromagnetic module (EMM)), datasets collected during different propagation experiments carried out in France [31, 32], Italy [13], Portugal [33], Spain [34], Svalbard, [35] Norway [36, 37], and French Guiana [38] are used. Their main geographical [39] (latitude, longitude, and altitude) and geometrical (elevation angle) characteristics are presented in Table 2.

The first database is constituted of propagation measurements collected in Southern France by ONERA from the 20.2 GHz beacon of ASTRA-3B satellite located at  $23.5^\circ$  East longitude on the geostationary orbit in two locations: Toulouse and Salon de Provence in 2014 [32]. Toulouse is situated in South-Western France. It is subject to both Atlantic and Mediterranean climatic influences. Salon de Provence is located at 294 km from Toulouse in South-Eastern France and is subject to the Mediterranean climatic influence. The data processing methodology is detailed in the study of Boulanger et al. [31].

The second dataset considered in this analysis is the statistics of excess attenuation collected in Aveiro (Western Portugal) in 2014 by Universidade de Aveiro from the

TABLE 2: Main geographical and geometrical characteristics of the 1-year experiments considered in this analysis.

Location	Longitude	Latitude	Altitude	Elevation angle
Toulouse	1.5°E	43.6°N	150 m	35.1°
Salon de Provence	5.1°E	43.6°N	67 m	36.4°
Aveiro	8.65°W	40.6°N	18 m	39.6°
Madrid	3.7°W	40.5°N	630 m	40.2°
Spino d'Adda	9.5°E	45.4°N	84 m	37.7°
SvalSat	15.4°E	78.2°N	495 m	2.65°
Kourou	52.7°W	5.2°N	0 m	78.5°

19.7 GHz beacon of the EUTELSAT Ka-Sat satellite located at 9°E in GEO orbit. As reported in the studies of Amaya et al. and Garcia et al. [33, 34], Aveiro is affected by an oceanic climate. Data processing methodology is detailed in the study of Amaya et al. [33].

The third dataset considered in this analysis is the statistics of excess attenuation collected in Madrid (central Spain) from September 2013 to August 2014 by Universidad Politécnica de Madrid from the 19.7 GHz beacon of Ka-Sat. Madrid is surrounded by mountains. It is located at an altitude of 630 m and is affected by a rather dry continental climate [34]. Data processing methodology is detailed in the study of Garcia et al. [34].

The fourth dataset considered in this analysis is the statistics of excess attenuation collected in Spino d'Adda (Northern Italy) in 1994 by Politecnico di Milano from the 18.7 GHz beacon of the ITALSAT F1 satellite located at 13.2°E in GEO orbit. As reported in the study of Riva [13], being near Milano, Spino d'Adda is affected both by the Mediterranean influence and the proximity of the Alps Mountain Range. Data processing methodology is detailed in the study of Riva [13].

The fifth dataset considered in this paper is constituted of statistics of total attenuation collected in a polar region at the satellite teleport (SvalSat) operated by KSAT in the Spitzbergen Island of the Svalbard archipelago in Norway. The measurements were collected by NASA from April 2016 to March 2017, from the 20.2 GHz beacon of the THOR 7 satellite located at 1°W in the GEO orbit and have been processed and analyzed by ONERA. As reported in the study of Houts et al. [36], two main characteristics have to be considered: on the one hand the climate is very dry because Svalbard lies on the polar circle, and on the other hand, the path length is very long because of the elevation angle lower than 3°. Data processing methodology is detailed in the study of Queyrel et al. [37].

The final dataset considered in this paper is the statistics of excess attenuation collected in an equatorial area at the Guiana Space Centre in Kourou (French Guiana) in 2018 by CNES from the 20.2 GHz beacon of the Amazonas 3 GEO satellite located at 61°W, as reported in the study of Boulanger et al. [38], Kourou is in a coastal area, subject to an equatorial climate in a relatively flat area without any tropical forest, with the main influence of the Atlantic Ocean. Data processing methodology is detailed in the study of Boulanger et al. [38].

Table 3 gathers the mean climatological normals for each experimental site considered in this study.

#### 4. Comparisons with Statistics Computed from Propagation Measurements

Comparisons with annual statistics are carried out firstly from propagation measurements collected in Toulouse in 2014, secondly from data measured in different locations in Southern Europe in Aveiro, Madrid, Salon de Provence, and Spino d'Adda, and thirdly for more specific climates at high latitude in Svalbard and at low latitude in Kourou.

Since the final temporal resolution obtained with WRF-EMM is 5 minutes, all experimental time series considered in this study have been undersampled to 5 minutes too. As a consequence, some differences may appear between the experimental results presented here and those published in the studies of Riva et al., Boulanger et al., Lacoste et al., and Garcia et al. [13, 31, 32, 34]. All annual statistics of rain attenuation presented in this section are plotted for time percentages between 0.01% and 5%. The lowest limit is chosen to get a sufficient number of samples to achieve meaningful results, i.e., ~10 points for the 5 min time step. The highest limit is chosen because it corresponds more or less to the probability of occurrence of rain in midlatitude European climates. For Svalbard, as total attenuation is considered, the plots are provided up to 100% of an average year.

*4.1. Comparisons with Propagation Measurements Collected at 20 GHz in Toulouse.* In a first step, simulations performed with WRF-EMM are compared with respect to propagation measurements collected in Toulouse from the 20.2 GHz beacon of ASTRA-3B. To illustrate the temporal behavior of the model, two examples of time series measured and generated with WRF-EMM are shown in Figure 4.

In both examples presented in Figure 4, the model is not able to reproduce accurately the instantaneous temporal variation of rain attenuation observed on the measurements, even if the rainy period is well identified especially in Figure 4(b). This can be explained either by the lower spatial resolution of the model ( $2 \times 2 \text{ km}^2$ ) or in time (one sample every 5 min). Another possible explanation is that the model is able to generate the expected rain events over a large area but not exactly where they are in reality within a few kilometres (as for any forecast model). Therefore, the following analysis will focus on the statistical representativeness of the model instead of the instantaneous temporal behavior.

To appreciate the ability of WRF-EMM to reproduce the statistical behavior of the atmospheric propagation channel, one full year of data simulated at 20.2 GHz in the direction of ASTRA-3B is generated with WRF-EMM for the year 2014. The configuration of the model is the one described in Section 2.

The statistics computed from the time series generated with WRF-EMM and obtained from the measurements are presented in Figure 5. They are compared to the CCDF predicted with Recommendation ITU-R P.618-13, taking as

TABLE 3: Annual mean climatological normals (1981–2010) for the experiments considered in this analysis.

Location	Temperature (min-max)	Rain amount	No. of rainy days
Toulouse	9.1/18.5°C	638.3 mm	96
Salon de Provence	8.7/20°C	579.3 mm	57
Porto (85 km/Aveiro)	10.0/18.8°C	1141.0 mm	106
Madrid	7.6/20.6°C	383.5 mm	58
Milano	7.8/17.1°C	920.1 mm	83
Longyearbyen airport	-46.3/21.7°C	271 mm	86
Kourou	23.4/30.2°C	2838 mm	191

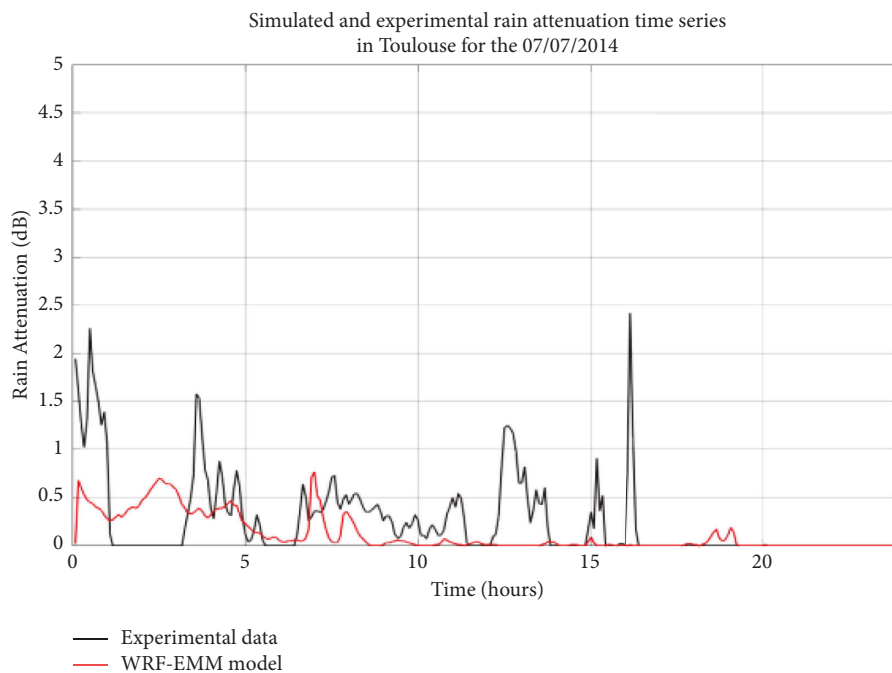
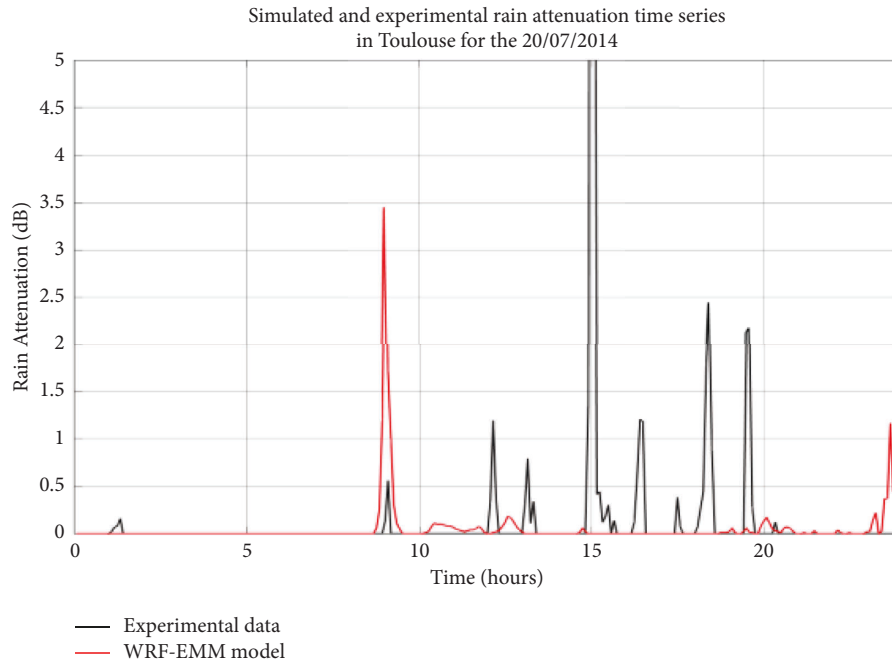


FIGURE 4: Examples of time series generated with WRF-EMM and measured in Toulouse from the 20.2 GHz beacon of ASTRA-3B on 20/07/2014 (a) and on 7/07/2014 (b).

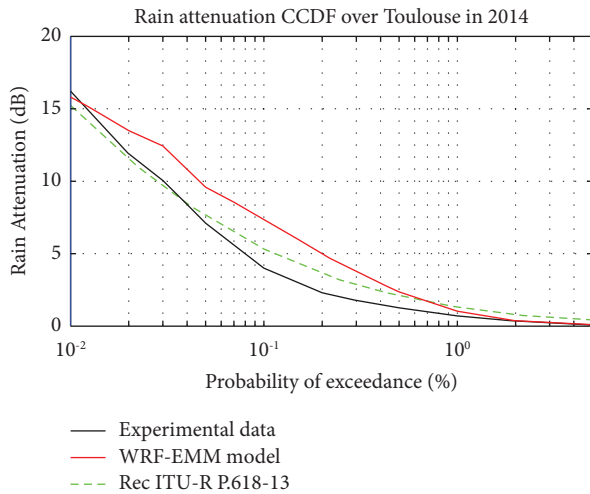


FIGURE 5: Comparisons between CCDFs computed from measurements collected in Toulouse in 2014 (99.2% availability (Figures 5 and 6, the availability refers to the percentage of valid measured attenuation time series over the full measurement period)), WRF-EMM simulations and Rec. ITU-R P.618-13 using  $R_{0,01}$  predicted with Rec. ITU-R P.837-7.

input the rainfall rate exceeded for 0.01% of an average year predicted by Recommendation ITU-R P.837-7.

Figure 5 shows that for this particular year the annual CCDF derived from one year of WRF-EMM simulations is higher than the measured and predicted CCDF for time percentages lower than 0.5%. For the highest time percentages above 0.5%, better results are obtained with WRF-EMM which is able to predict very well the probability to have rain attenuation on the link where Recommendation ITU-R P.618-13 fails due to the shape of the theoretical distribution in Step 10 of this model. Nevertheless, over the range of probability as a whole, the differences between the two approaches are small.

**4.2. Comparisons with Annual Attenuation Statistics in Aveiro, Madrid, Salon de Provence, and Spino d'Adda.** To broaden the discussion, in this section, the WRF-EMM simulator is tested against the other measured datasets listed in Section 3 in terms of annual statistics.

Results are presented in the following figures, for Aveiro (Figure 6), Madrid (Figure 7), Salon de Provence (Figure 8), and Spino d'Adda (Figure 9).

In Figure 6, the results obtained with the simulations are worse than the predicted ones using Recommendation ITU-R P.618-13 for almost all the considered time percentages, even if the shape of the statistics is better respected. A small bias seems to be present on the simulation that may be due to the coastal situation of this experiment. Indeed, the pixel considered on the one hand from ERA Interim to initialize WRF, and on the other hand as output of the WRF-EMM simulation is located both over the Atlantic Ocean and over lands.

In the case of Madrid which is affected by a continental climate, both the prediction and the simulation fail to reproduce the shape of the CCDF, even if the differences are

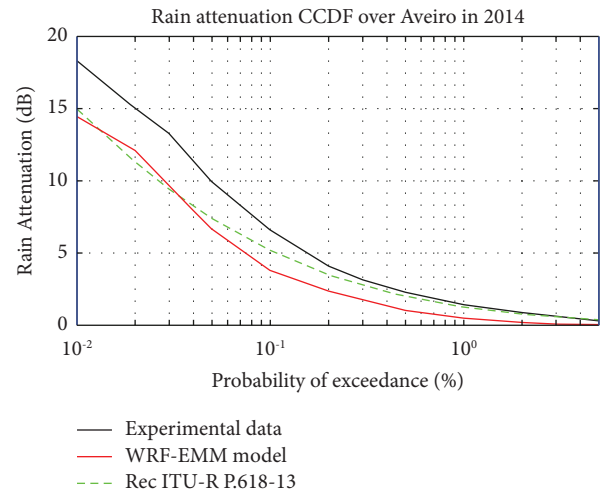


FIGURE 6: Comparisons between CCDFs computed from data measured in Aveiro in 2014 (99.1% availability), WRF-EMM simulations and Rec. ITU-R P.618-13 using  $R_{0,01}$  predicted with Rec. ITU-R P.837-7.

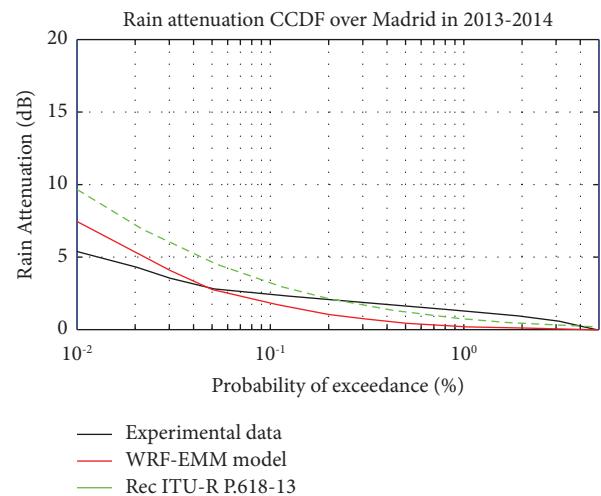


FIGURE 7: Comparisons between CCDFs computed from data measured in Madrid in 2013-14 (97.9% availability), WRF-EMM simulations and Rec. ITU-R P.618-13 using  $R_{0,01}$  predicted with Rec. ITU-R P.837-7.

not so high in absolute values in compliance with Figure 7. For this particular very dry year (between September 2013 and August 2014), WRF-EMM provides better results for percentages lower than 0.1%, whereas Recommendation ITU-R P.618-13 performs better above this time percentage.

For Salon de Provence, differently from Madrid, the measured CCDF is one of the worst cases ever measured at 20 GHz in Europe, which is confirmed by Météo France outlining very strong convective events called “Cevennes episodes” in this area during autumn 2014. Even if the estimate of the probability of rain attenuation and even if the shape of the statistics coming from the simulations performed with WRF-EMM are similar to the observations, further analyses need to be performed to better reproduce the particular strong convective events observed in 2014 in this area.

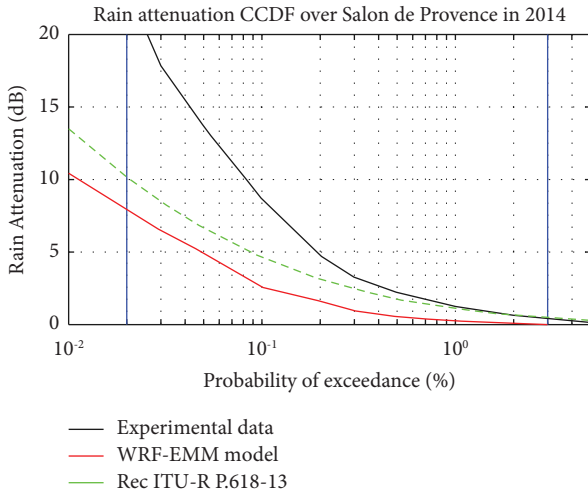


FIGURE 8: Comparisons between CCDFs computed from data measured in Salon de Provence in 2014 (94.7% availability), WRF-EMM simulations and Rec. ITU-R P.618-13 using  $R_{0.01}$  predicted with Rec. ITU-R P.837-7.

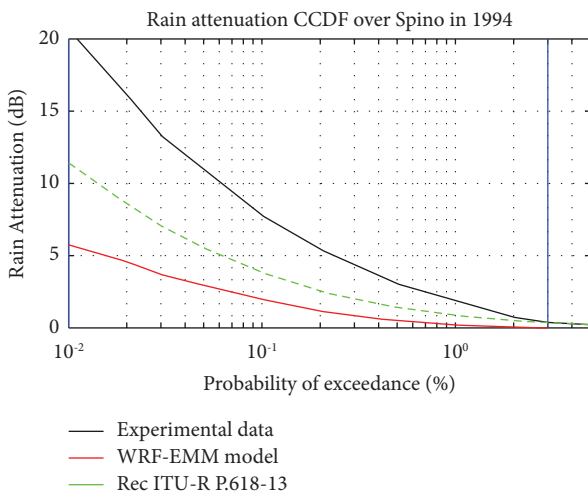


FIGURE 9: Comparisons between CCDFs computed from data measured in Spino d'Adda in 1994 (98.3% availability), WRF-EMM simulations and Rec. ITU-R P.618-13 using  $R_{0.01}$  predicted with Rec. ITU-R P.837-7.

The last comparison is achieved with respect to propagation data collected at 18.7 GHz in Spino d'Adda. Here, a similar trend as in Salon de Provence is observed, with better results obtained with Recommendation ITU-R P.618-13. However, here again, the simulated results obtained with WRF-EMM are not too far from the predicted ones.

**4.3. Comparisons with Annual Attenuation Statistics in Specific Climates at Low and High Latitudes.** In this section, specific climatic conditions are considered to reinforce the interest of using high resolution weather forecast models: on the one hand, a low latitude area with an equatorial climate

in French Guiana, and on the other hand, a high latitude area with a polar climate in Svalbard.

In a first step, the results of a similar analysis carried out for an equatorial area [39] from one year of propagation measurements collected in Kourou (French Guiana) [38] are presented in Figure 10.

For this equatorial area, quite good results are obtained with WRF-EMM for time percentages higher than 0.05%. In this case, the atmospheric simulator performs much better than Recommendation ITU-R P.618-13 fed with  $R_{0.01}$  predicted with Rec. ITU-R P.837-7.

In a second step, results are presented for the specific configuration of a very low elevation link ( $2.65^\circ$ ) at high latitude ( $78^\circ\text{N}$ ) in Svalbard. Considering this very specific geometry, rain attenuation is not the dominant effect to be taken into account, so unlike the results presented in this paper, the analysis has been carried out considering here total attenuation. In this specific configuration, the ray bending effect is taken into account using Recommendation ITU-R P.676-11.

The statistics of total attenuation in Svalbard computed from measurements, from the simulations with WRF-EMM and from Recommendations ITU-R P.618-13 for rain attenuation, P.840-8 for cloud attenuation and P.676-11 for gaseous attenuation are presented in Figure 11 for the period April 2016-March 2017 [37].

From the study of Houts et al.[36], here, both WRF-EMM and Recommendation ITU-R P.618-13 predict a CCDF a bit far from the measured one. However, for WRF-EMM simulations, there is an underprediction with respect to the measurements that could be explained by two missing effects: on the one hand by the absence of the impairments due to other hydrometeors than rain in this version of WRF-EMM, and on the other hand, by the specific configuration of this experiment with a very low elevation less than  $3^\circ$ , for which other contributions such as refraction and scintillation may play a more significant role than for usual elevation angles.

Eventually, the results presented in this section are an illustration of the potential of physical simulators based on meteorological models for link configurations for which the prediction method of rain attenuation recommended by ITU-R was not tested during its development (due to lack of corresponding data). For such cases, it can be expected that an atmospheric simulator relying on a high-resolution weather forecast model can provide fair results because of its physical nature.

**4.4. Quantitative Comparisons with the ITU-R Metric.** In this section, the annual rain attenuation statistics obtained by WRF-EMM model as well as the prediction method of Rec. ITU-R P.618-13 are compared to the experimental data from a quantitative point of view. For this purpose, the ITU-R metric described in Rec. ITU-R P.311-15 is used [35]. This metric is defined by the following step-by-step methodology:

- (1) Define a probability vector  $\mathbf{p}$  with  $N$  probabilities such as  $\mathbf{p} = (\mathbf{p}_i)_{i \in [1, N]}$  with  $\mathbf{p}_i \in [0.001\%, 0.002\%, 0.003\%, 0.005\%, 0.01\%, \dots, 100\%]$



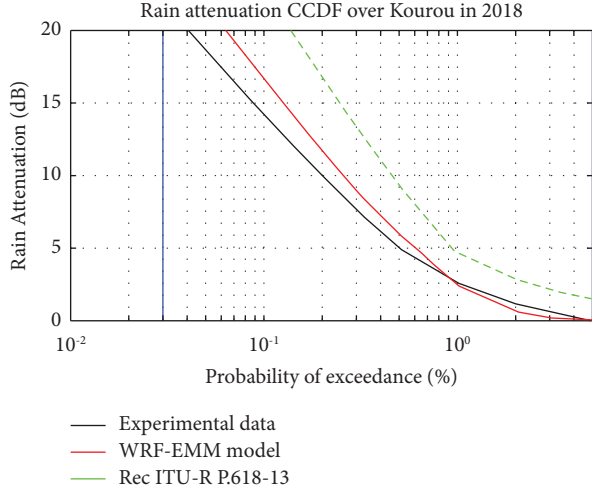


FIGURE 10: Comparisons between CCDFs computed from data measured in Kourou in 2018 (99.7% availability), WRF-EMM simulations and Rec. ITU-R P.618-13 using  $R_{0.01}$  predicted with Rec. ITU-R P.837-7.

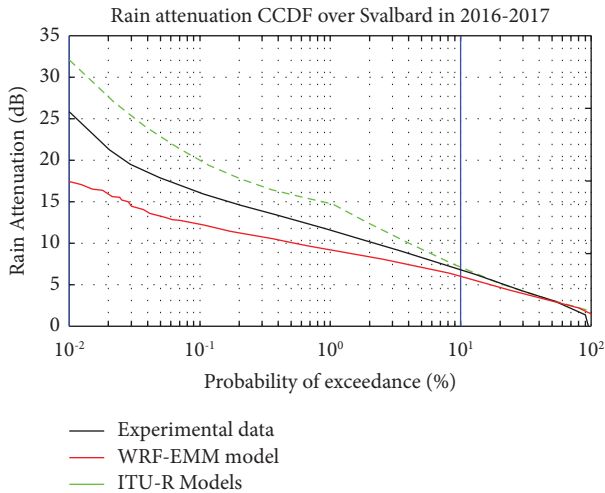


FIGURE 11: Comparisons between CCDFs of total attenuation computed from data measured in SvalSat in April 2016–March 17 (91.7% availability), WRF-EMM simulations and Rec. ITU-R P.618-13 using  $R_{0.01}$  predicted with Rec. ITU-R P.837-7, as well as Recommendations ITU-R P.840-8 and P.676-11.

- (2) Compute the  $\epsilon_{\text{ITUE},i}$  metric for every probability  $\mathbf{p}_i$  with  $A_{m,i}$  the measured attenuation and  $A_{p,i}$  the predicted attenuation such as

-if  $A_{m,i} < 10$  dB:

$$\epsilon_{\text{ITUE},i} = M \left( \frac{A_{m,i}}{10} \right)^{0.2} \ln \left( \frac{A_{p,i}}{A_{m,i}} \right). \quad (8)$$

-If  $A_{m,i} > 10$  dB:

$$\epsilon_{\text{ITUE},i} = M \ln \left( \frac{A_{p,i}}{A_{m,i}} \right), \quad (9)$$

TABLE 4: ITU metric error analysis between results obtained from WRF-EMM simulations and from Rec. ITU-R P.618-13.

Location	WRF-EMM mean error	WRF-EMM RMSE	P.618-13 mean error	P.618-13 RMSE
Toulouse	0.25	0.32	0.25	0.33
Salon	-1.79	1.83	-0.97	1.01
Aveiro	-0.57	0.64	-0.15	0.19
Madrid	-0.50	0.77	0.05	0.35
Spino d'Adda	-1.34	1.34	-0.49	0.55
Kourou	0.00	0.24	0.51	0.52
SvalSat	-0.24	0.25	0.19	0.20

with  $M$ , a weighing factor representing the number of years upon which the measured data is based on.

- (3) Calculate the final error  $\epsilon_{\text{ITUE},i}$ :

$$\epsilon_{\text{ITUE}} = \sqrt{\epsilon_{\text{ITUE},m}^2 + \epsilon_{\text{ITUE},s}^2}, \quad (10)$$

with

$$\epsilon_{\text{ITUE},m} = \frac{1}{N} \sum_i^N \epsilon_{\text{ITUE},i}, \quad (11)$$

and

$$\epsilon_{\text{ITUE},s} = \sqrt{\frac{1}{N} \sum_i^N (\epsilon_{\text{ITUE},i} - \epsilon_{\text{ITUE},m})^2}. \quad (12)$$

In this study, the probability vector  $\mathbf{p}$  is created with only certain probabilities considered as valid. For each location, the valid probabilities are illustrated on Figures 5–11 by blue vertical lines.

For the purpose of this analysis, both the mean error  $\epsilon_{\text{ITUE},m}$  and the RMSE  $\epsilon_{\text{ITUE},s}$  are calculated and are gathered in Table 4.

## 5. Conclusion

This paper has investigated the interest of using a high-resolution mesoscale weather forecast model coupled with a physical deterministic model to simulate the statistical behavior of rain attenuation affecting satellite communications at Ka-band. More specifically, Version 3.4 of the WRF-ARF weather forecast model initialized with the ECMWF ERA-Interim reanalysis database has been run to generate every five minutes the state of the troposphere crossed by the considered Earth-space links. The physical deterministic method used to convert the volume of the troposphere into propagation parameters and more particularly into rain attenuation relies on the Mie scattering theory considering a Marshall–Palmer rain drop size distribution.

Unlike other papers published on the use of high-resolution weather forecast models for propagation purposes that provide comparisons about specific rain events in

specific locations, this article focuses both on long-term simulations over a full period of one year as well as on several locations at mid latitudes and at high latitudes in Europe and in an equatorial area.

One year of simulations has been carried out to simulate time series of rain attenuation and then to compute the corresponding statistics. Several locations in different climates have been considered where rain attenuation measurements were available over one full year: in Toulouse and Salon de Provence (France), Aveiro (Portugal), Madrid (Spain), Spino d'Adda (Italy), SvalSat (Svalbard, Norway), and Kourou (French Guiana).

The comparisons between the simulated and the measured annual statistics provide encouraging results, the accuracy obtained with the simulator being on the same order of magnitude as the ones predicted with the reference prediction method of Recommendation ITU-R P.618–13 for the five midlatitude European locations considered in this paper. The observed significant differences are probably due to attenuation values generated by the model averaged over an entire pixel, which should be lower than the point measurements over the slant path. For the two specific climates at a high latitude in Svalbard and at a low latitude in French Guiana, significantly better results are obtained with the atmospheric numerical simulator based on the WRF high-resolution model, probably because the conventional prediction methods have not been developed and tested for these specific climates and configurations.

Therefore, at this stage, this paper demonstrated that this type of mesoscale weather forecast models is a promising solution to generate the behavior of the propagation channel, not only in clear sky conditions but also for precipitating systems to assess rain attenuation annual statistics, for a wide variety of climates. Time series generation using WRF models might be useful for predicting rain attenuation in order to develop fade mitigation techniques, so any future endeavour in this direction would be useful. In the future after more intense validation activities, the goal will be to exploit this kind of atmospheric numerical simulator to generate the statistical behavior of the propagation channel where measurements are not available. More precisely, this could be particularly interesting for specific geometrical configurations (such as for MEO or LEO satellite paths), low elevations, specific areas where orography plays a significant role, higher frequencies (such as V or W bands), or specific climatic areas for instance in the tropics.

However, work still needs to be done in order to improve the accuracy of the results. Different axes can be followed to reach this objective. The primary step is to consider a more recent version of the WRF weather forecast model (version 4) and to initialize it with more recent reanalysis databases such as ERA5 from the ECMWF which is characterized by higher spatial and temporal resolutions than ERA Interim ( $0.25^\circ \times 0.25^\circ$  instead of  $0.75^\circ \times 0.75^\circ$  in the space domain and 1 hour instead of 6 hours in the time domain).

The analysis presented in this paper was performed by propagation researchers that are not experts of weather forecast models. Therefore, the WRF model has been used

with the standard configuration recommended by its designers. In the future, the activity on the configuration of the model itself needs to be undertaken, considering for instance the number of domains to be considered in the simulation, the radiative transfer, and cumulus schemes or the microphysics of precipitation systems in terms of rain drop granulometry. More precisely, if the raindrop size distribution of Marshall–Palmer seems to be appropriate at midlatitudes, its applicability to tropical and equatorial regions as well as to high latitudes is more questionable.

## Data Availability

Statistical distributions of the data generated with the WRF-EMM atmospheric simulator of ONERA can be accessible on request to laurent.castanet@onera.fr.

## Conflicts of Interest

The authors declare that they have no conflicts of interest.

## Acknowledgments

The authors would like to thank Armando Rocha from University of Aveiro, José Manuel Riera from Universidad Politécnica de Madrid, and Carlo Riva from Politecnico di Milano for the access to the statistics of excess attenuation considered in this article. The analysis on French Guiana has been carried out in the CNES R&T study R–S15/TC-005-066 “Realization of a Ka-band propagation experiment in French Guiana.” The analysis on Svalbard has been done in the ESA study n°ESTEC 4000114488/15/NL/LvH: “Test-bed for channel Modelling in EO KA-Band DDL Systems,” carried out by KSAT, NASA, and ONERA, with additional support from CNES. This activity has been performed in the framework of a collaborative project (PIC PERF) cofunded by ONERA and CNES.

## References

- [1] H. Fenech, A. Tomatis, S. Amos, V. Soumpholphakdy, and J. L. Serrano Merino, “Eutelsat HTS systems,” *International Journal of Satellite Communications and Networking*, vol. 34, no. 4, pp. 503–521, 2016.
- [2] A. Kyrgiazos, B. Evans, P. Thompson, P. T. Mathiopoulos, and S. Papahalabos, “A terabit/second satellite system for European broadband access: a feasibility study,” *International Journal of Satellite Communications and Networking*, vol. 32, no. 2, pp. 63–92, 2014.
- [3] E. Cianca, T. Rossi, A. Yahalom, Y. Pinhasi, J. Farserotu, and C. Sacchi, “EHF for satellite communications: the new broadband frontier,” *Proceedings of the IEEE*, vol. 99, no. 11, pp. 1858–1881, November 2011.
- [4] C. Sacchi, T. Rossi, M. Murrioni, and M. Ruggieri, “Extremely high frequency (EHF) bands for Future broadcast satellite services: opportunities and challenges,” *IEEE Transactions on Broadcasting*, vol. 65, no. 3, pp. 609–626, September 2019.
- [5] R. Barnett, “O3b – a different approach to Ka-band satellite system design and spectrum sharing,” in *Proceedings of the ITU Regional Seminar for RCC Countries on Prospects for Use*

- of the Ka-Band by Satellite Communication Systems, Almaty, Kazakhstan, September 2012.
- [6] M. Schuman, "Oneweb presentation," in *Proceedings of the ITU Symposium And Workshop*, Barcelona, Spain, November 2017.
  - [7] E. Salonen, S. Karhu, P. Jokela et al., "Modelling and calculation of atmospheric attenuation for low-fade margin satellite communications," *ESA Journal*, vol. 16, no. n<sup>o</sup>3, pp. 299–316, 1992.
  - [8] R. Itu, *Propagation Data And Prediction Methods Required For The Design Of Earth-Space Telecommunication Systems*, Recommendation ITU-R P.618-13, Geneva, Switzerland, 2017.
  - [9] L. Castanet, J. Lemorton, and M. Bousquet, "Fade mitigation techniques for new satcom services at ku-band and above: a review," in *Proceedings of the 4th Ka-Band Utilization Conference*, Venice, Italy, November 1998.
  - [10] R. Itu, "Time series synthesis of tropospheric impairments," in *Proceedings of the Recommendation ITU-R P.1853-2*, Geneva, Switzerland, August 2019.
  - [11] R. K. Crane, X. Wang, D. B. Westenhaver, and W. J. Vogel, "ACTS propagation experiment: experiment design, calibration, and data preparation and archival," *Proceedings of the IEEE*, vol. 85, no. 6, pp. 863–878, June 1997.
  - [12] Opex, "Reference book on attenuation," in *Proceedings of the 2nd Workshop Of the OLYMPUS Propagation Experimenters (OPEX), Doc. ESA-ESTEC-WPP-083 Volume 1*, Noordwijk, Netherlands, November 1994.
  - [13] C. Riva, "Seasonal and diurnal variations of total attenuation measured with the ITALSAT satellite at Spino d'Adda at 18.7, 39.6 and 49.5 GHz," *International Journal of Satellite Communications and Networking*, vol. 22, no. 4, pp. 449–476, 2004.
  - [14] C. Riva and A. Martellucci, "Preface to the special issue on the Alphasat Aldo Paraboni propagation experiment," *International Journal of Satellite Communications and Networking*, vol. 37, no. 5, pp. 385–386, 2019.
  - [15] Y. Karasawa and Y. Maekawa, "Ka-Band Earth-Space propagation Research in Japan," *Spec. issue on Ka-band propagation effects on Earth-satellite links, Proceedings of the IEEE*, vol. 85, no. 6, pp. 821–842, 1997.
  - [16] D. D. Hodges, R. J. Watson, and G. Wyman, "An attenuation time series model for propagation forecasting," *IEEE Transactions on Antennas and Propagation*, vol. 54, no. 6, pp. 1726–1733, 2006.
  - [17] V. Fabbro, N. Jeannin, K. Djafri, J. Lemorton, and D. Vanhoenacker-Janvier, "Scintillation modelling in troposphere using multiple phase screen," in *Proceedings of the ESA Workshop on Radiowave Propagation 2011, ESTEC*, Noordwijk, Netherlands, December 2011.
  - [18] M. Outeiral-Garcia, N. Jeannin, L. Feral, and L. Castanet, "Use of WRF Model to Characterize Propagation Effects in the Troposphere," in *Proceedings of the 7th European Conference on Antennas and Propagation*, Gothenburg, Sweden, April 2013.
  - [19] M. Biscarini, F. S. Marzano, M. Montopoli et al., "Optimizing data volume return for ka-band deep space links exploiting short-term radiometeorological model forecast," *IEEE Transactions on Antennas and Propagation*, vol. 64, no. 1, pp. 235–250, 2016.
  - [20] N. Jeannin, M. Outeiral-Garcia, L. Castanet et al., "Atmospheric channel simulator for the simulation of propagation impairments for ka band data downlink," in *Proceedings of the Eighth European Conference On Antennas And Propagation*, La Hague, Netherlands, April 2014.
  - [21] L. Quibus, L. Luini, C. Riva, and D. Vanhoenacker-Janvier, "Use and accuracy of numerical weather predictions to support EM wave propagation experiments," *IEEE Transactions on Antennas and Propagation*, vol. 67, no. 8, pp. 5544–5554, 2019.
  - [22] G. Fayon, L. Feral, L. Castanet, N. Jeannin, and X. Boulanger, "Use of WRF to Emulate Site Diversity Schemes in South of France," in *Proceedings of the XXXIIInd General Assembly And Scientific Symposium Of the International Union of Radio Science*, Montréal (Québec, Canada), August 2017.
  - [23] W. C. Skamarock, J. B. Klemp, J. Dudhia et al., *A Description of the Advanced Research WRF Version 3*, NCAR, Boulder, CO, USA, 2008.
  - [24] D. P. Dee, S. M. Uppala, A. J. Simmons et al., "The ERA-interim reanalysis: configuration and performance of the data assimilation system," *Quarterly Journal of the Royal Meteorological Society*, vol. 137, no. 656, pp. 553–597, 2011.
  - [25] T. Manabe, T. Ihara, and Y. Furuhashi, "Inference of raindrop size distribution from attenuation and rain rate measurements," *IEEE Transactions on Antennas and Propagation*, vol. 32, no. 5, pp. 474–478, 1984.
  - [26] K. L. S. Gunn and T. W. R. East, "The microwave properties of precipitation particles," *Quarterly Journal of the Royal Meteorological Society*, vol. 80, no. 346, pp. 522–545, 1954.
  - [27] P. S. Ray, "Broadband complex refractive indices of ice and water," *Applied Optics*, vol. 11, no. 8, pp. 1836–1844, 1972.
  - [28] C. W. Ulbrich and D. Atlas, "Rainfall microphysics and radar properties: analysis methods for drop size spectra," *Journal of Applied Meteorology*, vol. 37, no. 9, pp. 912–923, 1998.
  - [29] J. S. Marshall and W. McK. Palmer, "The distribution of raindrops with size," *Journal of Meteorology*, vol. 5, no. 4, pp. 165–166, 1948.
  - [30] H. C. Hulst and H. C. van de Hulst, *Light Scattering by Small Particles*, Courier Corporation, North Chelmsford, USA, 1981.
  - [31] X. Boulanger, B. Gabard, L. Casadebaig, and L. Castanet, "Four years of total attenuation statistics of earth-space propagation experiments at ka-band in Toulouse," *IEEE Transactions on Antennas and Propagation*, vol. 63, no. 5, pp. 2203–2214, 2015.
  - [32] X. Boulanger, F. Lacoste, and L. Castanet, "Small and large scale site diversity experiment at ka-band in the South of France," *International Journal of Satellite Communications and Networking*, vol. 36, no. 1, pp. 14–28, 2018.
  - [33] C. Amaya, T. Nguyen, A. Rocha et al., "Joint results of long-term Earth-space propagation experiments at 20-GHz in Canada and Europe," *Space Communications*, vol. 22, no. 2-4, pp. 81–89, 2013.
  - [34] J. M. Garcia-Rubia, J. M. Riera, P. Garcia-del-Pino, G. A. Siles, and A. Benarroch, "Experimental assessment of slant-path rain attenuation variability in the Ka-band," *International Journal of Satellite Communications and Networking*, vol. 34, no. 2, pp. 155–170, 2016.
  - [35] R. Itu, "Fascicle on testing variables used for the selection of prediction methods," <https://www.itu.int/en/ITU-R/study-groups/rsg3/Pages/fascicles.aspx>.
  - [36] J. R. Houts, J. A. Nessel, and M. J. Zemba, "Design of a Ka-band propagation terminal for atmospheric measurements in polar regions," in *Proceedings of the 2016 10th European Conference on Antennas and Propagation (EuCAP)*, pp. 1–3, Davos, Switzerland, April 2016.
  - [37] J. Queyrel, X. Boulanger, L. Castanet et al., "Preliminary Results of the THOR7 Propagation Experiment in the North

- Pole Region,” in *Proceedings of the 25th Ka and Broadband Communications Conference*, Sorrento, Italy, October 2019.
- [38] X. Boulanger, B. Benammar, and L. Castanet, “Propagation experiment at ka-band in French Guiana: first year of measurements,” *IEEE Antennas and Wireless Propagation Letters*, vol. 18, no. 2, pp. 241–244, 2019.
- [39] V. Le Mire, X. Boulanger, L. Castanet, B. Benammar, and L. Feral, “Potentialities of the numerical weather prediction model wrf to produce attenuation statistics in tropical regions,” in *Proceedings of the 2020 14th European Conference on Antennas and Propagation (EuCAP)*, Copenhagen, Denmark, March 2020.